



ELSEVIER

Available online at www.sciencedirect.com

SCIENCE @ DIRECT®

Surface Science 530 (2003) 37–54

SURFACE SCIENCE

www.elsevier.com/locate/susc

Adsorption of NH₃ on oxygen pre-treated Ni(1 1 1)

E. Laksono, A. Galtayries *, C. Argile, P. Marcus

Laboratoire de Physico-Chimie des Surfaces CNRS (UMR 7045), Université Pierre et Marie Curie, Ecole Nationale Supérieure de Chimie de Paris, 11 rue Pierre et Marie Curie, F-75005 Paris, France

Received 14 November 2002; accepted for publication 25 January 2003

Abstract

The adsorption of NH₃ on oxygen pre-treated Ni(1 1 1) surfaces has been studied at room temperature using X-ray photoelectron spectroscopy (XPS). Oxygen pre-treatments have been performed at 650 K. This protocol leads to a “two-phase domain” (O-adsorbed phase + NiO islands) over a large range of oxygen exposures. The investigation of the surface reactivity towards NH₃ shows that ammonia is adsorbed provided that the O-adsorbed phase is present; the surface reactivity increases with the O-adsorbed phase coverage. Two N-adspecies have been detected from the N 1s core level peaks at 399.8 ± 0.2 and 397.8 ± 0.2 eV and assigned to molecular NH₃ and dissociated NH₂ species, respectively. The molecular adsorption results from direct impingement of the NH₃ molecules, whereas the dissociated one results from the dissociation of a part of the preadsorbed molecular species. At saturation, the dissociated species is the more abundant one (about 4/5 of the total N 1s peak) whatever the initial coverage (>0) of the surface by the O-adsorbed phase. The XPS data indicate that this dissociation is correlated to the formation of OH from oxygen of the adsorbed phase and hydrogen abstraction from the molecular ammonia. When the O-adsorbed phase is absent on the surface, i.e. for clean Ni(1 1 1) or the complete NiO layer, none of these surface reactions with ammonia occurs, under the same adsorption conditions.

© 2003 Elsevier Science B.V. All rights reserved.

Keywords: Chemisorption; Ammonia; Low index single crystal surfaces; Nickel; Nickel oxides; Oxygen; X-ray photoelectron spectroscopy

1. Introduction

Over the past three decades, the adsorption and decomposition of ammonia on metals, as well as on metal oxide layers, has attracted much interest. Structural techniques as well as electronic and

vibrational spectroscopies have been used. Studies of this system cover model surfaces (single crystals of metals, or metal oxide layers on metal single crystals) as well as more complex ones (polycrystalline metals, oxide layers on metallic polycrystals), on which molecular or dissociative adsorption of ammonia can occur over a wide range of temperatures. In all cases, understanding of the mechanisms of ammonia interaction with the surfaces is essential. There are important applications in more complex processes, for example in heterogeneous catalysis, where ammonia is either a reactant (for

* Corresponding author. Tel.: +33-1-44276737; fax: +33-1-46340753.

E-mail address: anouk-galtayries@enscp.jussieu.fr (A. Galtayries).



example the industrial synthesis of HNO_3 by ammonia oxidation over a platinum catalyst—known as “Ostwald process”—or the HCN synthesis, by reaction of methane with ammonia and oxygen over a platinum–rhodium catalyst—known as “Andrussow process”) or a product (for example the industrial synthesis of NH_3 from nitrogen and hydrogen over an iron catalyst—known as “Haber–Bosch process”—or the undesirable production of ammonia in the automotive exhaust gas converter) or even the catalyst (NH_3 -catalysed sequential surface reactions [1]). Another example is the corrosion of metals in the presence of atmospheric pollutants such as ammonia. Surface nitridation for semiconductor applications may also be mentioned [2–7]. Finally, NH_3 is an often used probe molecule for investigating the acidity of solid surfaces [8].

The studies of the chemisorption of ammonia on metal surfaces published up to the early eighties (1984) have been reviewed by Lambert and Bridge [9]. The major part of the surface studies of NH_3 adsorption in the eighties were focused on the well-defined surfaces of transition or noble metals [10–15], at low temperature of adsorption between about 100 and 200 K. The question of non-dissociative versus dissociative adsorption behaviour, and the structure of the surface ammonia complexes were investigated by different electronic and vibrational spectroscopies as well as by thermal desorption measurements. As we will not focus our work on the NH_3 adsorption on metals, we only briefly summarise here that, depending on the metal, the NH_3 ability to dissociate is strongly decreasing from the left hand side to the right hand side of the transition metal series. A more complete picture of the NH_3 adsorption on various metals at the end of this period was given by Thornburg and Madix [16] in 1989. From experimental work, it has been shown that in the molecular state, ammonia molecules bond with their nitrogen end nearest to the surface, and their C_{3v} symmetry axis normal to the surface. This bonding has been interpreted as implying that nitrogen donates its lone pair of electrons to the surface to form the bond to the metal. However, according to theoretical work of the time (late eighties), the bonding is mostly electrostatic in nature, involving

the permanent dipole of ammonia and an induced dipole in the surface. It was stated in this work [16] that the binding site of ammonia was not unambiguously established for any of the quoted single crystal surfaces, and different electropositive sites have been proposed implying both models of bonding: electron donation of the nitrogen lone pair to the metal as well as electrostatic bonding on the surface. Recently, an interesting bibliographic review of the previous research on NH_3 adsorption on Ni(110) has been published by Chrysostomou et al. [17]. The authors also raised the problem of the stability of molecularly-adsorbed ammonia when probing with photons or electrons, as early suggestions on the decomposition pathways of ammonia on Ni(110) have been later questioned (see in Ref. [17]). In particular, Jaeger et al. [18] have provided clear evidence for the occurrence of photon-induced reduction of ammonia on Ni(110) during surface characterisation. Nevertheless, surface analysis techniques employing electron irradiation (LEED, Auger, HREELS...) and temperature-programmed desorption (TPD or TD) have been found to be even more damaging to the integrity of the adsorbed ammonia than those based on photon irradiation. All logical dehydrogenated intermediates expected to form during the surface decomposition of ammonia: $\text{NH}_2(\text{ads})$, $\text{NH}(\text{ads})$, $\text{N}(\text{ads})$ have been proposed on Ni(110). However, there is some disagreement in the literature on the exact mechanism of ammonia decomposition and on the intermediates involved in the decomposition.

Despite the large number of works carried out during the eighties, several fundamental questions are still debated in the more recent surface science literature on the ammonia interaction with metals: the interactions of ammonia with Rh(111) [19] have been studied at low pressure whereas the attention was previously focused on the decomposition of ammonia in moderate pressure conditions only; the interactions of NH_3 with Ru(001) [20], Pt(111) [21,22], the multilayer coverage on Ag(111) [23], the interaction of ammonia with nickel single crystals studied by more recent techniques as angle-resolved photoemission extended fine-structure spectroscopy (ARPEFS) on Ni(100)

Ni(111) surfaces, as a function of the initial oxygen exposure, investigated by XPS.

2. Experimental

For the XPS characterisations, Ni 2p, O 1s and N 1s core level spectra have been recorded with a VG ESCALAB Mk II X-ray photoelectron spectrometer, with an un-monochromatised AlK α anode, at a pass energy of 20 eV. The binding energies were referenced to the Ni 2p $_{3/2}$ line and Au 4f $_{7/2}$, set at 852.8 and 84.0 eV, respectively, and given with an accuracy of 0.1 eV for intense spectra and 0.2 eV for less intense signals corresponding to low coverage adspecies (N 1s, O 1s). Clean and O-treated surfaces were also checked from contamination by recording a survey spectrum and the C 1s and S 2p core level spectra. The spectra of the surfaces prior to ammonia adsorption were characterised at electron take-off angles of 90° with respect to the sample surface. Connected to the UHV analysis chamber (base pressure 3×10^{-10} Torr) of the spectrometer is a UHV preparation chamber (base pressure 5×10^{-10} Torr) with heating and gas introduction facilities. The Ni(111) surface was cleaned by cycles of Ar $^+$ sputtering and annealing, first in H $_2$ and then in vacuum. This sequence was found to be the best compromise, in our experiments, to avoid both S segregation due to prolonged annealing under vacuum and oxygen or carbon re-contamination. After cleaning the surface, high purity oxygen and ammonia (from Air Liquide) were introduced in the treatment chamber. Oxygen exposures were typically performed at $P_{O_2} = 1 \times 10^{-6}$ mbar (1×10^{-7} mbar for the two lower O $_2$ exposures). The O-pre-treated Ni(111) samples have been exposed to ammonia at room temperature, at 1×10^{-7} mbar. Ammonia was typically admitted for periods of 3 min in the preparation chamber, after which the gas was evacuated and the sample analysed by XPS in the analysis chamber. Exposures in the preparation chamber are reported in langmuirs (L) ($1 \text{ L} = 10^{-6}$ Torr · s). Note that the reported pressures and exposures, in the text or in the figure captions, are not corrected for ion gauge sensitivity. The sample temperature, during oxygen ex-

posures, was measured with a pyrometer. To analyse the individual contributions of the Ni 2p $_{3/2}$, O 1s, and N 1s core levels, peak decomposition was carried out with a computer program using gaussian/lorentzian peak shapes, and a Shirley background.

3. Results and discussion

3.1. Oxygen interaction on Ni(111) at 650 K prior to NH $_3$ exposure

At room temperature, and up to 500 K, it is usually accepted (see, for example [40] and references therein) that O $_2$ interaction with Ni(111) proceeds via three steps: (i) a rapid chemisorption ending with a first plateau, (ii) a second increase in oxygen uptake correlated with the nucleation and growth of NiO islands and then (iii) the formation of a full oxide layer, leading to a second plateau. Up to the end of the first plateau, it is established [41] that chemisorption occurs with little effects on the core level spectra, which indicates that the surface atoms retain their metallic character. At room temperature, this chemisorption stage gives rise to a p(2 × 2) structure for a maximum coverage of 1/4 of a monolayer. At coverages above ~0.28 ML, some authors report a ($\sqrt{3} \times \sqrt{3}$)R30° structure, and some do not (see, for example, [40] and references therein). Raising the temperature above ~300 K causes the ($\sqrt{3} \times \sqrt{3}$)R30° structure (when observed) to convert to a split p(2 × 2) [40]. In the domain where the NiO formation occurs, the Ni core level spectra reflect the occurrence of the oxide nucleation and passive oxide film formation. The mechanisms currently accepted for the oxidation involve the nucleation and growth of oxide islands within the O-adsorbed phase. The growth is expected to occur at the perimeter of the oxide nuclei with oxygen supplied by surface diffusion [40,42]. It has been proposed that, up to 473 K [40], the hexagonal, kinetically favoured NiO(111) structure grows rapidly to coalescence covering the entire Ni(111) surface. At higher temperature ($T > 473$ K), NiO(100) starts to form irreversibly, indicating that this is the thermodynamically favoured form of the oxide also on

hydroxylated NiO islands were the minor component.

As indicated above, in the frequent controversy between OH(a) and O(a) or O⁻ binding energies, the assignment of binding energy of the O(a) species remains questionable. We performed another type of test to check the possibility of an OH contribution. A clean Ni(1 1 1) sample was treated in O₂ at room temperature, and subsequently exposed to water vapour at room temperature. The O 1s region clearly showed a significant increase of the high binding energy contribution located at 531.5 ± 0.2 eV that we attributed to the presence of hydroxyl groups on the surface.

In our series of experiments it comes out that, after oxidation at 650 K, the O 1s core level peaks present an hydroxyl contribution at 531.5 ± 0.2 eV, corresponding to about 10% of the total O 1s peak area. According to a previous work [46], this surface hydroxylation likely corresponds to the NiO(1 1 1) grains, which are the minor components of the NiO film at high temperature, as NiO(1 0 0) starts to form irreversibly above 473 K [40]. It has been also noted that for the lower O₂ exposures (corresponding to values of the XPS intensity ratio $I(\text{O})_{\text{total}}/I(\text{Ni})_{\text{total}}$ below 0.04), the surface hydroxylation is more important. This unexpected result may be related to the experimental conditions: the lowest exposures were performed at $P_{\text{O}_2} = 1 \times 10^{-7}$ mbar (instead of 1×10^{-6}) so that the partial pressure of residual water was proportionally higher.

The data obtained for various oxygen exposures are presented in Fig. 1: the XPS intensity ratio $I(\text{O})_{\text{total}}/I(\text{Ni})_{\text{total}}$, obtained from the integration of the O 1s and Ni 2p_{3/2} core levels, is plotted as a function of the O₂ exposure expressed in langmuirs (L). In Fig. 1, a first plateau (corresponding to the oxygen adsorption phase) is not evidenced, as compared with what is reported in the literature [40]. This is not related with the temperature of adsorption: literature data show that the higher the temperature of adsorption, the longer is the first plateau in the oxygen uptake curve. This might be attributed to a lack of data at the lowest oxygen exposures, but it is more likely correlated with our experimental protocol: oxygen exposures and sample heating in the preparation chamber,

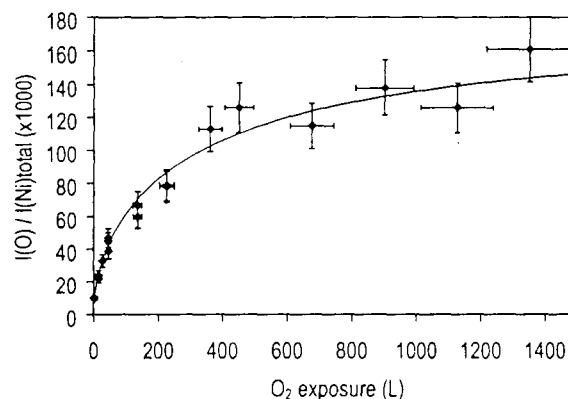


Fig. 1. O 1s intensity (normalised with respect to the Ni 2p_{3/2} core level intensity) as a function of oxygen exposure (expressed in Langmuir) at 650 K.

and XPS measurements in the analysis chamber. Indeed, the different surface compositions were “frozen” in the preparation chamber, by stopping the sample heating, but the temperature decrease was not instantaneous. Simultaneously, oxygen was pumped away. However the pressure decrease was gradual, so the true O₂ exposure is always slightly higher than indicated. Consequently, not all of the exposure was performed at constant temperature and pressure, so our results cannot be directly compared with the literature data at $T \leq 500$ K. Moreover, a change in the surface layer structure during the sample cooling cannot be excluded: it has been shown that thin oxide films, formed on Ni(1 1 1) at 500 K, decompose rapidly under annealing at 550 K [47].

To investigate the role of oxygen in the interaction of NH₃ with Ni(1 1 1), it appeared necessary to characterize the NiO growth mode in our experimental protocol, using our XPS data. For this purpose, we have considered two main hypotheses: either the oxide formation proceeds via a “layer-by-layer” growth mode or it corresponds to a “two-phase domain” (nucleation and growth of NiO island among the O-adsorbed phase), as in the kinetic conditions between 300 and 500 K. In this approach, the Ni 2p_{3/2} core levels have been decomposed systematically into the metallic and Ni²⁺ (in NiO) features, and the oxidic contribution at 529.8 eV has been extracted from the O 1s core level

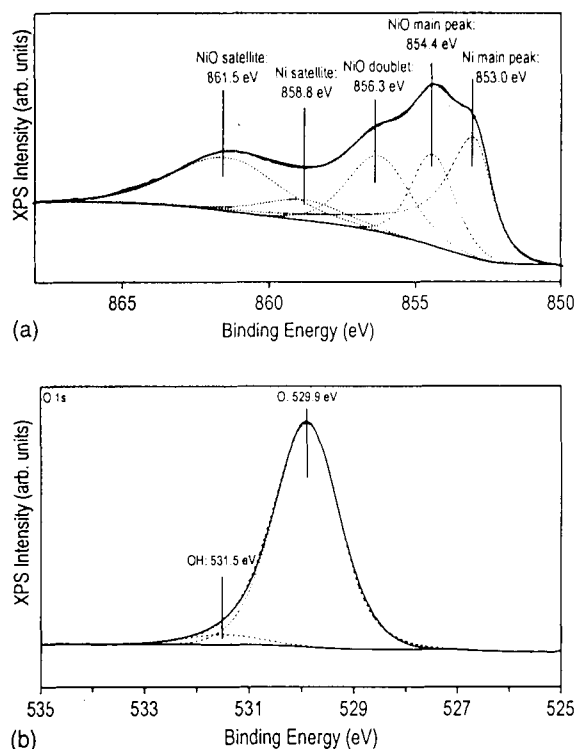


Fig. 2. (a) Ni 2p_{3/2} and (b) O 1s core level peaks decomposition into the metallic and oxide (NiO) features, after 450 L of exposure of O₂ with Ni(1 1 1) at 650 K.

16.2 Å for O in the (100)-oriented oxide ($\lambda_{\text{O}}^{\text{NiO}(100)}$). It was assumed that the attenuation of the nickel signal through an O-adsorbed monolayer can be neglected, and thus $\exp(-d''/\lambda_{\text{Ni}}^{\text{O}} \sin \beta) \approx 1$. For both models, the following ratios have been used:

$$\frac{I(\text{O})_{\text{oxide}}^{\infty}}{I(\text{Ni})_{\text{oxide}}^{\infty}} = 0.223, \quad \frac{I(\text{Ni})_{\text{oxide}}^{\infty}}{I(\text{Ni})_{\text{metal}}^{\infty}} = 0.815$$

and

$$\frac{I(\text{O})_{\text{adsorbed phase}}^{\text{monolayer}}}{I(\text{O})_{\text{oxide}}^{\infty}} = 0.049$$

Details on the calculations are reported in the Appendix. In Fig. 3a and b, calculated and experimental values of $I(\text{O})_{\text{oxide}}/I(\text{Ni})_{\text{oxide}}$ have been superimposed. One can easily observe that the “layer-by-layer” model does not fit the data, whereas the “two-phase domain” model provides a satisfactory fit. Other values of $\lambda_{\text{M}}^{\text{N}}$, derived from

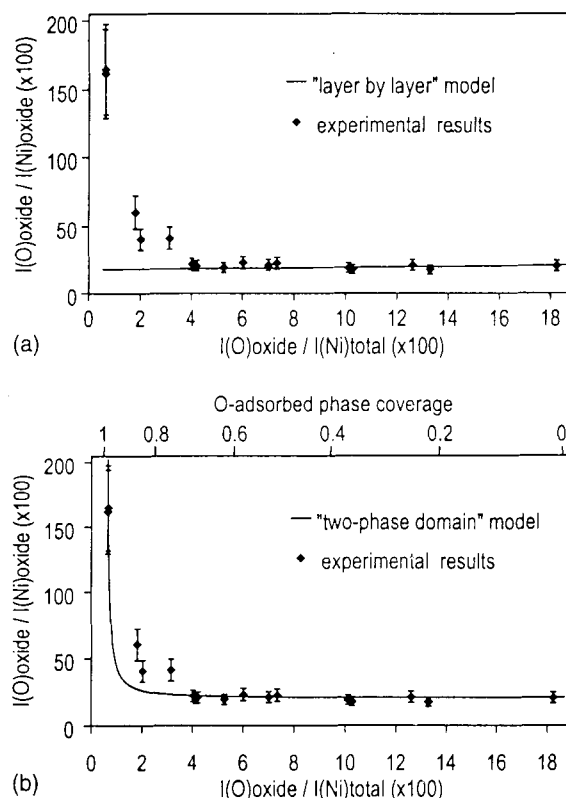


Fig. 3. (a) O/Ni²⁺ XPS intensity ratio, obtained from the O 1s core level and the Ni 2p_{3/2} core level for Ni²⁺ in NiO, as a function of the total O/Ni XPS intensity ratio, obtained from the O 1s and Ni 2p_{3/2} core levels. Points: experimental results; full line: layer-by-layer model. (b) O/Ni²⁺ XPS intensity ratio, obtained from the O 1s core level and the Ni 2p_{3/2} core level for Ni²⁺ in NiO, as a function of the total O/Ni XPS intensity ratio, obtained from the O 1s and Ni 2p_{3/2} core levels. Points: experimental results; full line: two-phase domain model.

more recent equations [49,50], have been tested: they induce changes in the calculated thickness of the nickel oxide layer but the shape of the curves (Fig. 3a and b) remains unchanged. The main reason for the small deviation of some experimental points most probably comes from the too simplistic hypothesis of the isomorphic growth of the oxide islands in the very early stages of the NiO growth. We conclude that the two-phase domain model described well the growth of the NiO oxide layer, in our experimental conditions, and this result will be used for the following NH₃ adsorption studies.

3.2. NH_3 adsorption

In the present work, adsorption of ammonia on clean and oxygen pre-treated Ni(1 1 1) surfaces was performed at room temperature, in the preparation chamber of the spectrometer. A typical controlled exposure of ammonia lasts 3 min at the desired pressure. At the end of the treatment, ammonia is pumped down to a pressure of 10^{-8} mbar, and the sample is transferred to the analysis chamber for XPS measurements. The sample can then be re-exposed to ammonia under the same conditions.

In the absence of oxygen on the Ni(1 1 1) surface, no adsorption of NH_3 was observed by XPS, in agreement with previous data [39]. After interaction of ammonia with the oxygen pre-treated Ni(1 1 1) samples, two N-adspecies have been detected in the N 1s core level region: one located at 399.8 ± 0.2 eV and the other one at 397.8 ± 0.2 eV. All N 1s core level spectra have been systematically decomposed into a combination of these two features. For a low NH_3 exposure (13.5 L), if the XPS analysis is performed just after the exposure to ammonia, the N 1s core level presents a main feature at high binding energy (HBE: 399.8 eV). If the same analysis is repeated after one night in UHV, the ratio between the surface adspecies is significantly changed in favour of the low-binding energy adspecies (LBE: 397.8 eV). The situation is different for cumulated NH_3 exposures from 40.5 L up to about 180 L: the N 1s core level presents a main feature at LBE and the XPS spectra remain unchanged with time in the analysis chamber.

To focus on the initial stages of adsorption for low ammonia exposures, the O-pre-treated Ni(1 1 1) samples were exposed to NH_3 for 13.5 L in the preparation chamber, then the N 1s signal was measured as a function of time in UHV, during about 500 min. The same procedure was repeated four times. Fig. 4 shows a typical series of N 1s spectra obtained as a function of time in UHV after exposure to NH_3 (XPS ratio $I(\text{O})_{\text{total}}/I(\text{Ni})_{\text{total}} = 0.022$). Each N 1s core level peak has been decomposed into a combination of the LBE and HBE components. Fig. 5 shows the results obtained as a function of time, for the two adspecies and for the total N 1s signal. After the first

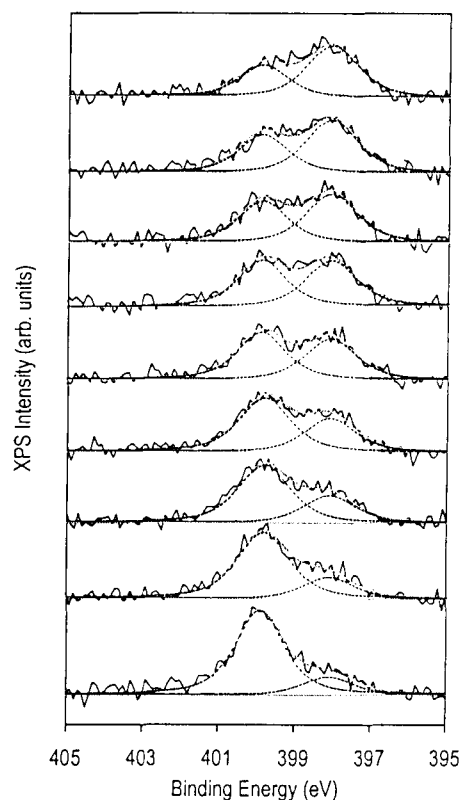


Fig. 4. Changes in the N 1s spectrum as a function of time in UHV, after the first NH_3 exposure of 13.5 L at room temperature. The N 1s peak decomposition into the HBE and LBE components is shown. The Ni(1 1 1) substrate was pre-treated by O_2 at 650 K, 30 seconds at 1×10^{-7} mbar. From the first (lower part) to the fourth spectrum, as well as from the fifth to the last spectrum (upper part), the time between two spectra is 45 min. Between the fourth and fifth spectra, this time is 90 min. The total time scale is ~ 9 h.

exposure to ammonia, the low BE signal increases with time whereas the high BE signal decreases. Moreover, the total NH_3 uptake decreases with time, suggesting a partial desorption of the high BE adspecies. After the second ammonia exposure, the observations are similar, with a less pronounced increase in the low BE signal. After the third dose, the surface distribution between the HBE and LBE N 1s features remains almost unchanged with respect to the last N 1s spectrum recorded after the second dose. However, the total N 1s area has slightly increased compared to the second dose. No further change is observed after

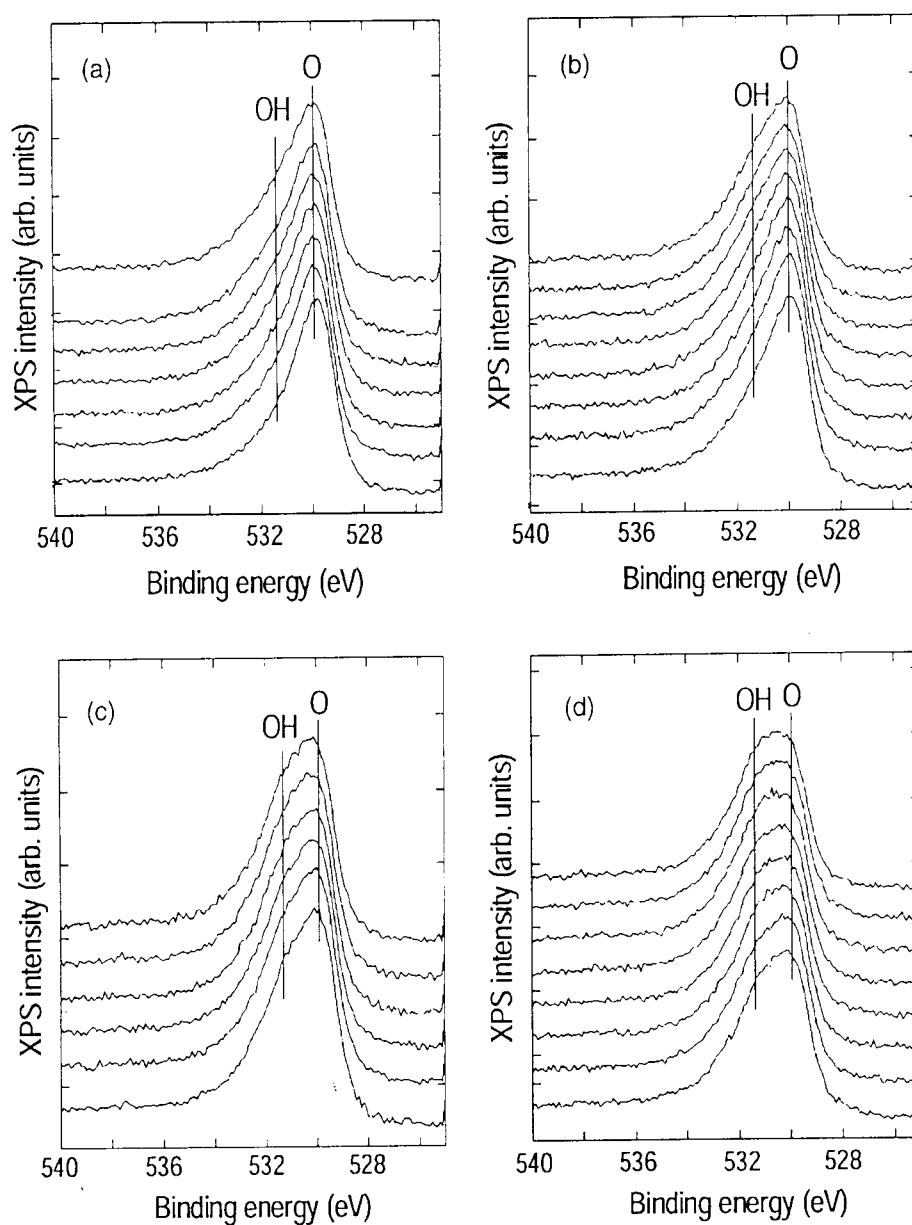


Fig. 9. Changes in the O 1s spectrum as a function of time in UHV obtained after (a) the first ammonia exposure (13.5 L), (b) the second ammonia exposure (13.5 L), (c) the third ammonia exposure (13.5 L), (d) the fourth ammonia exposure (13.5 L). Between the first (bottom) spectrum and the last (top) spectrum, the time scale is: ~ 6 h for the first exposure (a), ~ 8 h for the second exposure (b), ~ 7 h for the third exposure (c) and ~ 8 h for the fourth exposure (d).

intensity ratios of these surfaces after the mentioned treatments.

After annealing under UHV, the Ni 2p_{3/2} core level peak exhibits a main feature corresponding to

metallic nickel, larger than before annealing, and the O 1s core level peak area is less intense, with a shoulder at 531.5 eV, less pronounced compared to the spectrum before annealing. From these ob-

Table 1
XPS intensity ratios obtained from the O 1s and Ni 2p_{3/2} core levels after O₂ interaction at 650 K, before and after UHV annealing at 650 K

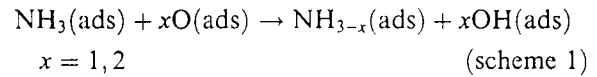
	Thin film 1 $I(\text{O})_{\text{total}}/I(\text{Ni})_{\text{total}}$	Thin film 2 $I(\text{O})_{\text{total}}/I(\text{Ni})_{\text{total}}$
Before annealing	0.15	0.13
After annealing	0.12	0.05

servations on the core levels, different hypotheses can be considered involving a decrease in the quantity of nickel oxide and/or a decrease in the oxide surface coverage: (i) either a decrease in the oxide islands thickness, the oxide coverage remaining constant; or (ii) a decrease in the oxide coverage, the oxide islands thickness being constant; or (iii) a decrease in the coverage of oxide with an increase of the oxide island thickness; or (iv) both a decrease in the oxide coverage and the oxide thickness.

As regards the surface reactivity towards ammonia, it was observed in both cases that the adsorption was greatly enhanced compared to the surface before annealing. For Thin Film 1, corresponding to $I(\text{O})_{\text{total}}/I(\text{Ni})_{\text{total}} = 0.12$ (see Table 1), the XPS intensity ratio after ammonia adsorption becomes $I(\text{N})/I(\text{Ni})_{\text{total}} = 9 \times 10^{-4} \pm 1 \times 10^{-4}$ and for thin film 2, the ratio is $I(\text{N})/I(\text{Ni})_{\text{total}} = 14 \times 10^{-4} \pm 1 \times 10^{-4}$. Based on our previous observation of the absence of reactivity of nickel oxide in our conditions (Fig. 7), this new series of experiments confirms the enhanced reactivity of the O-adsorbed phase on the surface of the sample. In the particular case of Thin Film 1, in spite of a small decrease of the XPS ratio $I(\text{O})_{\text{total}}/I(\text{Ni})_{\text{total}}$ (from 0.15 to 0.12), the ammonia adsorption enhancement suggests a decrease in the coverage of oxide with an increase of the oxide island thickness (hypothesis (iii)): not only the NiO(100) phase decomposed into the O-adsorbed phase but also a local thickening of the oxide islands occurred, as already observed with Ni substrates (100)-oriented [52].

At this point, to summarise the results, we have observed that NH₃ reacts with the Ni(111) surface provided some O-adsorbed phase is present; once adsorbed, molecular NH₃ reacts with oxygen to form dissociated ammonia species and hydroxyl

groups as a function of time, according to the following reaction:



The value of x will be discussed below.

3.3. Discussion

We first comment on the binding energies of the N-adsorbed species. In this work, two different values have been measured: the LBE at 397.8 ± 0.2 eV, and the HBE at 399.8 ± 0.2 eV. Some selected values of N 1s BE, from the literature, are reported in Table 2.

To focus more specifically on the comparison with previous works on ammonia adsorption at room temperature on oxygen pre-treated nickel single crystals, Grunze et al. [29] have already faced the difficulty of unambiguously identifying the nature of a NH₃ adsorption complex on an oxygen pre-covered Ni(100) surface. They observed a broad peak centred at 399.6 eV, but did not attempt to decompose it and assigned it to NH₃ or NH₂·HO. In the work of Kulkarni et al. [33] on oxygen pre-treated Ni(100) and Ni(110), the broad N 1s spectra obtained after ammonia exposure at 300 K, centred at 398.0 eV, were

Table 2
Comparison of N 1s BE for adsorbed nitrogen species on different metals and oxides

Adsorbed nitrogen species	N 1s BE (eV)	Reference
BN on Ni(100)	398.5	[53]
NH ₃ on Ni(110)	400.9	[13]
NH ₃ on Ni(100)	400.5	[33]
	400.2 and 399.8 (second layer)	[29]
NH ₃ on Ag(111)	400.1	[54]
NH ₃ on Cr ₂ O ₃ /Cr(110)	400.7	[38]
NH ₂ on different metals	398.7–399.4	[54]
NH ₂ on Cr ₂ O ₃ /Cr(110)	398.6	[38]
NH on different metals	398.0–398.6	[54]
NH _x ($x = 1, 2$) on Ni(100)	398.5	[33]
NH on Ni(100)	397.7	[29]
NH on Ni(110)	398.4	[13]
N on different metals	396.6–397.0	[54]
N on Ni(100)	397.0	[33]

minority of the O-adsorbed atoms are in states 3a (or 3b) and 3c. The majority of oxygen is in state 3d. Moreover, the extrapolation of the data of Fig. 5 to $t = 0$ indicates that about 20% of the molecular adsorbed ammonia has desorbed in UHV conditions. In state 2, the atomic O/NH₃ ratio can be roughly estimated to 4/1, which means that, even before the ammonia desorption and conversion stage, all the equivalent fcc hollow sites are not occupied by molecular ammonia. The possible electronic or steric effects hindering the adsorption of ammonia in some fcc sites are not elucidated.

It is to be noted that the first hypotheses (states 1 and 2) are the same as those put forward by Netzer and Madey [27], with adsorption in hollow sites. With the same sites for the O-adsorbed phase (state 1), another possibility would be to assign the molecular ammonia of state 2 to top sites, except the ones that are nearest to the adsorbed oxygen. This configuration leads to the same alternative for the NH₂ sites (states 3a and 3b in Fig. 10). Theoretical calculations might help in distinguishing which hypothesis is more likely.

4. Conclusions

The general features that can be derived from the above results are as follows.

As regards the interaction of oxygen with Ni(111) at 650 K, it was shown that, under our experimental conditions, the surface oxidation proceeds via a “two-phase domain”: O-adsorbed phase and NiO islands coexist in a large range of oxygen exposure.

As regards the surface reactivity towards NH₃, at room temperature and at 1×10^{-7} mbar, the conclusions are the following:

(i) There is no adsorption on the clean Ni(111) surface.

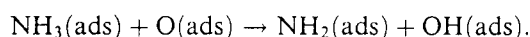
(ii) The surface reactivity is strongly correlated with the presence of O-adsorbed phase coverage: the higher the O_{ads} coverage, the higher the amount of adsorbed ammonia.

(iii) A continuous nickel oxide thin layer is not reactive in our conditions.

(iv) Two N-adspecies have been detected from the N 1s core level peak, at 399.8 ± 0.2 eV (high BE

feature) and at 397.8 ± 0.2 eV (low BE feature), and assigned to molecular NH₃ and dissociated NH_{x(x=1,2)} species, respectively.

(v) For low ammonia exposures, the dissociated ammonia adspecies is formed from a fraction of the molecular adspecies, and concomitantly, the hydroxyl component in the O 1s core level peak increases, while the main feature at 529.9 eV decreases. This simultaneous transformation has evidenced the hydrogen abstraction of ammonia by adsorbed oxygen to product OH and NH_x. A quantitative treatment of the XPS data gives the following stoichiometry:



(vi) From our experimental results, it appears that the kinetics of desorption of ammonia is faster than the kinetics of dissociation.

(vii) The total amount of adsorbed ammonia at saturation is about five times smaller than the amount of O-adsorbed species. At equilibrium, the ratio between molecular NH₃ and NH₂ adspecies is 1:4.

(viii) The behaviour of the two nitrogen adspecies suggests that two different adsorption sites are required.

Appendix

Calculation of the XPS intensity ratios for the “two-phase domain” and the “layer-by-layer” models

(1) The $I(\text{Ni})_{\text{oxide}}^{\infty}/I(\text{Ni})_{\text{metal}}^{\infty}$ and $I(\text{O})_{\text{adsorbed phase}}^{\text{monolayer}}/I(\text{O})_{\text{oxide}}^{\infty}$ XPS ratios are respectively expressed by:

$$\frac{I(\text{Ni})_{\text{oxide}}^{\infty}}{I(\text{Ni})_{\text{metal}}^{\infty}} = \frac{I(\text{Ni})_{\text{oxide}}^{\text{one layer}}}{I(\text{Ni})_{\text{metal}}^{\text{one layer}}} \frac{\left[1 - \exp\left(-\frac{t}{\lambda_{\text{Ni}}^{\text{oxide}} \sin \beta}\right)\right]}{\left[1 - \exp\left(-\frac{t}{\lambda_{\text{Ni}}^{\text{metal}} \sin \beta}\right)\right]}$$

and

$$\frac{I(\text{O})_{\text{adsorbed phase}}^{\text{monolayer}}}{I(\text{O})_{\text{oxide}}^{\infty}} = \frac{I(\text{O})_{\text{adsorbed phase}}^{\text{monolayer}}}{I(\text{O})_{\text{oxide}}^{\text{one layer}}} \times \left[1 - \exp\left(-\frac{t}{\lambda_{\text{O}}^{\text{NiO}} \sin \beta}\right)\right]$$

where: t is the thickness of one NiO(100) layer (= 2.086 Å) and t' is the thickness of one Ni(111) layer (= 2.036 Å).

Assuming that the photoelectron emission by one atom (cross section) is independent of its chemical environment, the

$$\frac{I(\text{Ni})_{\text{oxide}}^{\text{one layer}}}{I(\text{Ni})_{\text{metal}}^{\text{one layer}}} \quad \text{and} \quad \frac{I(\text{O})_{\text{adsorbed phase}}^{\text{monolayer}}}{I(\text{O})_{\text{oxide}}^{\text{one layer}}}$$

ratios are equivalent to the ratios of the number of atoms in one layer for each compound. For Ni(111)-oriented, NiO(100)-oriented and a p(2 × 2) O-adsorbed phase, we obtain

$$\frac{I(\text{Ni})_{\text{oxide}}^{\text{one layer}}}{I(\text{Ni})_{\text{metal}}^{\text{one layer}}} = 0.617 \quad \text{and} \quad \frac{I(\text{O})_{\text{adsorbed phase}}^{\text{monolayer}}}{I(\text{O})_{\text{oxide}}^{\text{one layer}}} = 0.405$$

which leads to

$$\frac{I(\text{Ni})_{\text{oxide}}^{\infty}}{I(\text{Ni})_{\text{metal}}^{\infty}} = 0.815 \quad \text{and} \quad \frac{I(\text{O})_{\text{adsorbed phase}}^{\text{monolayer}}}{I(\text{O})_{\text{oxide}}^{\infty}} = 0.049$$

(2) To obtain the $I(\text{O})_{\text{oxide}}^{\infty}/I(\text{Ni})_{\text{oxide}}^{\infty}$ ratio, we have used the general quantitative formula:

$$\frac{I(M)_N^{\infty}}{I(P)_N^{\infty}} = \frac{\sigma_M D_M^N \lambda_M^N T(KE)}{\sigma_P D_P^N \lambda_P^N T(KE)}$$

where: M , P are two different elements, N is the matrix formed by M and P , D is the atomic density of M or P in the matrix N , and σ is the Scofield cross section [51].

For the VG ESCALAB Mk II spectrometer, $\lambda_M^N T(KE)/\lambda_P^N T(KE)$ is constant, which leads to:

$$\frac{I(M)_N^{\infty}}{I(P)_N^{\infty}} \approx \frac{\sigma_M D_M^N}{\sigma_P D_P^N}$$

With $D_{\text{O}}^{\text{NiO}} = D_{\text{Ni}}^{\text{NiO}}$ (= 0.0916 mol/cm³), $\sigma_{\text{O}1s} = 2.93$ and $\sigma_{\text{Ni}2p_{3/2}} = 14.61$, the calculation leads to: $I(\text{O})_{\text{oxide}}^{\infty}/I(\text{Ni})_{\text{oxide}}^{\infty} = 0.20 \pm 0.03$, assuming an uncertainty of 5% on the values of σ mentioned by Scofield [51]. Within this range, the best fit between the experimental results and the theoretical model is obtained for $I(\text{O})_{\text{oxide}}^{\infty}/I(\text{Ni})_{\text{oxide}}^{\infty} = 0.22$.

References

- [1] J.W. Klaus, S.M. George, Surf. Sci. 447 (2000) 81.
- [2] J. Stober, B. Eisenhut, G. Rangelov, Th. Fauster, Surf. Sci. 321 (1994) 111.
- [3] A.A. Saranin, O.L. Tarasova, V.G. Kotljars, E.A. Khrantsova, V.G. Lifshits, Surf. Sci. 331–333 (1995) 458.
- [4] C. Bater, M. Sanders, J.H. Craig Jr., Surf. Sci. 451 (2000) 226.
- [5] V.M. Bermudez, Thin Solid Films 347 (1999) 195.
- [6] V.M. Bermudez, Chem. Phys. Lett. 317 (2000) 290.
- [7] H.L. Siew, M.H. Qiao, C.H. Chew, K.F. Mok, L. Chan, G.Q. Xu, Appl. Surf. Sci. 173 (2001) 95.
- [8] M. Kaltchev, W.T. Tysoc, Surf. Sci. 430 (1999) 29.
- [9] R.M. Lambert, M.E. Bridge, in: D.A. King, W.P. Woodruff (Eds.), The Chemical Physics of Solid Surfaces and Heterogeneous Catalysis, vol. 3B, Elsevier, Amsterdam, 1984, pp. 59–105.
- [10] C.W. Seabury, T.N. Rhodin, R.J. Purtell, R.P. Merrill, Surf. Sci. 93 (1980) 117.
- [11] C.R. Brundle, J. Vac. Sci. Technol. 13 (1976) 301.
- [12] K. Jacobi, E.S. Jensen, T.N. Rhodin, R.P. Merrill, Surf. Sci. 108 (1981) 397.
- [13] M. Grunze, M. Golze, R.K. Driscoll, P.A. Dowben, J. Vac. Sci. Technol. 18 (1981) 611.
- [14] B.A. Sexton, G.E. Mitchell, Surf. Sci. 99 (1980) 523.
- [15] G.B. Fisher, Chem. Phys. Lett. 79 (1981) 452.
- [16] D.M. Thornburg, R.J. Madix, Surf. Sci. 220 (1989) 268.
- [17] D. Chrysostomou, J. Flowers, F. Zaera, Surf. Sci. 439 (1999) 34.
- [18] R. Jaeger, J. Stöhr, T. Kendelewicz, Surf. Sci. 134 (1983) 547.
- [19] J.W. Niemantsverdriet, R.M. van Hardeveld, R.A. van Santen, Surf. Sci. 369 (1996) 23; R.M. van Hardeveld, R.A. van Santen, J.W. Niemantsverdriet, J. Vac. Sci. Technol. A 15 (1997) 1558.
- [20] W. Widdra, T. Moritz, K.L. Kostov, P. König, M. Staufer, U. Birkenheuer, Surf. Sci. Lett. 430 (1999) L558.
- [21] C. Bater, J.H. Campbell, J.H. Craig Jr., Thin Solid Films 340 (1999) 7.
- [22] Y. Shingaya, H. Kubo, M. Ito, Surf. Sci. 427–428 (1999) 173.
- [23] G.J. Szulczewski, J.M. White, Surf. Sci. 406 (1998) 194.
- [24] Y. Zheng, E. Moler, E. Hudson, Z. Hussain, D.A. Shirley, Phys. Rev. B 48 (1993) 4760.
- [25] K.-M. Schindler, V. Fritzsche, M.C. Asensio, P. Gardner, D.E. Ricken, A.W. Robinson, A.M. Bradshaw, D.P. Woodruff, J.C. Conesa, A.R. Gonzalez-Elipse, Phys. Rev. B 46 (1992) 4836.
- [26] I.C. Bassignana, K. Wagemann, J. Küppers, G. Ertl, Surf. Sci. 175 (1986) 22.
- [27] F.P. Netzer, T.E. Madey, Surf. Sci. 119 (1982) 422.
- [28] T.E. Madey, C. Benndorf, Surf. Sci. 152–153 (1985) 587.
- [29] M. Grunze, P.A. Dowben, C.R. Brundle, Surf. Sci. 128 (1983) 311.
- [30] C.T. Au, M.W. Roberts, Chem. Phys. Lett. 74 (1980) 472.
- [31] M.W. Roberts, Appl. Surf. Sci. 52 (1991) 133, and references therein.
- [32] B. Afsin, P.R. Davies, A. Pashusky, M.W. Roberts, D. Vincent, Surf. Sci. 284 (1993) 109.

- [33] G.U. Kulkarni, C.N.R. Rao, M.W. Roberts, *J. Phys. Chem.* 99 (1995) 3310.
- [34] H.E. Dastoor, P. Gardner, D.A. King, *Surf. Sci.* 289 (1993) 279.
- [35] L. Ruan, I. Stensgaard, E. Lægsgaard, F. Besenbacher, *Surf. Sci.* 314 (1994) L873.
- [36] M.-C. Wu, C.M. Truong, D.W. Goodman, *J. Phys. Chem.* 97 (1993) 4182.
- [37] R.S. Mackay, K.H. Junker, J.M. White, *J. Vac. Sci. Technol. A* 12 (1994) 2293.
- [38] H. Ma, Y. Berthier, P. Marcus, *Appl. Surf. Sci.* 153 (1999) 40.
- [39] A. Galtayries, E. Laksono, C. Argile, P. Marcus, *Surf. Interf. Anal.* 30 (2000) 140.
- [40] C.R. Brundle, J.Q. Broughton, in: D.A. King, W.P. Woodruff (Eds.), *The Chemical Physics of Solid Surfaces and Heterogeneous Catalysis*, vol. 3A, Elsevier, Amsterdam, 1990, pp. 351–370.
- [41] P.R. Norton, R.L. Tapping, *Faraday Disc. Chem. Soc.* 60 (1975) 71.
- [42] F. Besenbacher, J.K. Nørskov, *Prog. Surf. Sci.* 44 (1993) 5.
- [43] C.M. Kim, H.S. Jeong, E.H. Kim, *Surf. Sci.* 459 (2000) L457.
- [44] P. Finetti, M.J. Scantlebury, R. McGrath, F. Borgatti, M. Sambì, L. Zaratini, G. Granozzi, *Surf. Sci.* 461 (2000) 240.
- [45] F. Rohr, K. Wirth, J. Libuda, D. Cappus, M. Bäumer, H.-J. Freund, *Surf. Sci. Lett.* 315 (1995) L977.
- [46] N. Kitakatsu, V. Maurice, C. Hinnen, P. Marcus, *Surf. Sci.* 407 (1998) 36.
- [47] N. Kitakatsu, V. Maurice, P. Marcus, *Surf. Sci.* 411 (1998) 215.
- [48] M.P. Seah, *Auger and X-ray Photoelectron Spectroscopy, Practical Surface Analysis*, vol. 1, Wiley, Chichester, 1990, pp. 201–255.
- [49] P.J. Cumpson, M.P. Seah, *Surf. Interf. Anal.* 25 (1997) 430.
- [50] S. Tanuma, C.J. Powell, D.R. Penn, *Surf. Interf. Anal.* 25 (1997) 25.
- [51] J.H. Scofield, *J. Electron Spectrosc.* 8 (1976) 129.
- [52] R. Kubiak, H. Morgner, O. Rakhovskaya, *Surf. Sci.* 321 (1994) 229.
- [53] R.M. Desrosier, D.W. Greve, A.J. Gellman, *Surf. Sci.* 382 (1997) 35.
- [54] A.L. Schwaner, E.D. Pylant, J.M. White, *J. Vac. Sci. Technol. A* 14 (1996) 1453.
- [55] W. Biemolt, A.P.J. Jansen, M. Neurock, G.J.C.S. van de Kerkhof, R.A. van Santen, *Surf. Sci.* 287–288 (1993) 183.